Structural Analysis of Peptide Fragment 71–93 of Transthyretin by NMR Spectroscopy and Electron Microscopy: Insight into Amyloid Fibril Formation†

Jacqueline A. Jarvis, Sharon L. A. Munro, and David J. Craik*

School of Pharmaceutical Chemistry, Victorian College of Pharmacy (Monash University), 381 Royal Parade, Parkville, VIC, 3052 Australia

Received April 20, 1993; Revised Manuscript Received August 25, 1993®

ABSTRACT: A peptide corresponding to the amino acid region 71–93 of the plasma protein transthyretin (TTR) has been synthesized to investigate its role in the native folding of the molecule and the possible relationship between mutations in this region and amyloid formation of TTR. In the native structure this fragment includes a β-strand followed by a short helix and turns back on itself to form part of an antiparallel β-sheet. Electron microscopy has shown that the peptide is not intrinsically amyloidogenic. NMR spectroscopy has been used to investigate the conformational dependency of the peptide on the solution conditions. Minor populations of peptide showing partial turns were apparent in deuterated dimethyl sulfoxide (DMSO-d_6). Some indication of nascent helix between residues 5 and 12 was observed in water, and upon the addition of 20% trifluoroethanol (TFE) the span of helix was confirmed. The intrinsic tendency to form a helical structure between residues 5 and 12 in solution suggests that the helical region, also present in the native crystallographically determined TTR structure at corresponding residues 75–82, is an important folding initiation site. In contrast, the β-sheet motif observed in the native structure was not detected in solution. It is proposed that mutations in TTR occurring in the helical region result in subtle changes in the TTR structure leading to amyloid fibril formation.

The forces determining the folding, stabilization, and intermolecular interactions of proteins remain an intriguing central theme in structural biology. Interest has extended from native protein structure and activity to studies of folding intermediates and aggregation phenomena. NMR[1] spectroscopic studies of protein fragments have been used to elucidate specific structural aspects that are inherent in a particular amino acid sequence (Dyson & Wright, 1991). These can be used to identify regions of specific binding or sites in the protein important for directing the pathway of folding.

In the current study attention is focused on the amyloidogenic propensity of the plasma protein transthyretin (formerly called prealbumin). Transthyretin (TTR) is a 55-kDa nonglycosylated protein comprised of four identical 127-residue monomers (Figure 1). It is an exceptionally stable tetramer, remaining in a native conformation in the presence of 6 M urea (Branch *et al.*, 1972). Transthyretin serves as a serum carrier of thyroid hormones as well as retinol and retinol binding protein (RBP), and its three-dimensional structure has been well characterized using crystallographic techniques (Blake *et al.*, 1978). The subunits are approximately 50% β-sheet and contain one short region of helix. The monomers form dimers through an interaction stabilized by extensive hydrogen bonding between antiparallel strands of β-sheet. Two dimers assemble into a tetramer by opposing their inner β-sheets and interacting mainly at loop regions adjoining β-strands G and H and β-strands A and B.

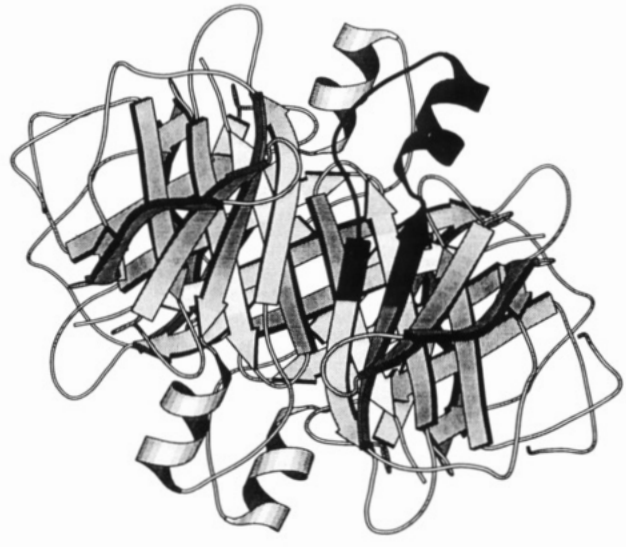

FIGURE 1: Molscript diagram (Kraulis, 1991) of the human transthyretin (TTR) tetramer (Blake et al., 1978). Highlighted is the fragment from residue 71 to residue 93 of one monomer. Crystal coordinates (entry 2pab 1.8, version of July 1992) were obtained from the Protein Data Bank at Brookhaven National Library (Bernstein *et al.*, 1977).

Transthyretin is one of several protein types which are able to form long β-sheet-based fibrillar structures of approximately 10-nm width and of indeterminant length. Such amyloid fibrils are often selectively deposited in renal, cardiac, or peripheral nerves, interfering with the function of these sites. The fibrils underlie a host of diseases including various forms of cancer, rheumatoid arthritis, type 2 diabetes, Alzheimer's disease, and specific polyneuropathies (Glenner, 1980). Transthyretin, TTR fragments, and variant TTR have all been identified in

† This work was supported in part by a grant from the Department of Employment, Education and Training.

* Author to whom correspondence should be addressed (telephone, 613 387 7222; facsimile, 613 389 9582).

® Abstract published in *Advance ACS Abstracts,* November 15, 1993.

[1] Abbreviations: NMR spectroscopy, nuclear magnetic resonance spectroscopy; NOE, nuclear Overhauser enhancement; NOESY, NOE spectroscopy; DQF-COSY, double-quantum-filtered correlation spectroscopy; TOCSY, total correlation spectroscopy; RMSD, root mean square deviation; SA, simulated annealing; 1D, one dimensional; 2D, two dimensional; TTR, transthyretin; ppm, parts per million; ppb, parts per billion; DSS, 4,4-dimethyl-4-silapentane-1-sulfonate; TFE, trifluoroethanol; $d_{\alpha N}(i,j)$, $d_{NN}(i,j)$, etc., intramolecular distance between the protons αH and NH, NH and NH, etc. on residues i and j; CD, circular dichroism.

0006-2960/94/0433-33$04.50/0 © 1994 American Chemical Society

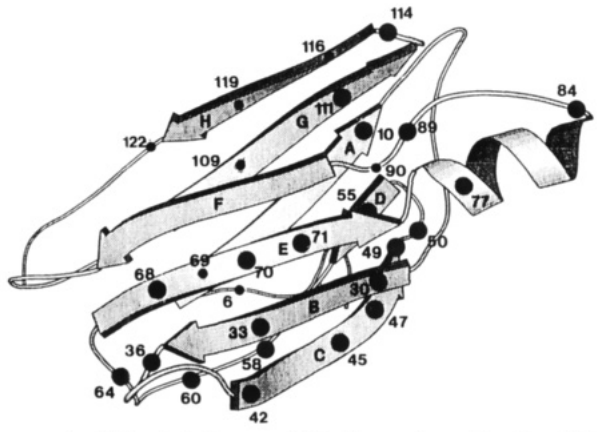

FIGURE 2: Molscript diagram of the human transthyretin (TTR) monomer showing positions of characterized mutations. The large circles represent mutations associated with amyloidosis, and the smaller circles represent positions of nonamyloidogenic mutations.

two general forms of amyloidosis: senile systemic amyloidosis and several familial amyloidoses (Westermark *et al.*, 1990; Colon & Kelly, 1992; Gafni *et al.*, 1985). It is not clear how the structural characteristics of transthyretin are altered so that the amyloid fibrils form and are then deposited with a specificity for peripheral and autonomic nerves or specific organs (Benson, 1991).

A recent finding suggests that the amyloidogenic behavior of TTR involves the improper interactions of inner cleft β-strands. The peptidic fragments of TTR corresponding to residues 10–20 and 105–115 (the A and G strands, respectively) have been shown to form amyloid-like structures *in vitro* (Gustavsson *et al.*, 1991). These hydrophobic regions show a great propensity for β-sheet-based fibril formation under several solution conditions and may be the main elements involved in the *in vivo* phenomena. Several mutant forms of TTR associated with familial amyloidosis have been identified, as have benign forms and variants associated with other abnormalities. These have been summarized by Terry et al. (1993) in a study of the Met 30 variant of TTR. The positions of the mutations causing amyloidosis occur in different regions of the molecule (Figure 2), indicating that amyloid formation may involve several mechanisms. The amyloidogenic mutants still form functional TTR tetramers—both in homogeneous and heterogeneous transthyretin preparations (Refetoff *et al.*, 1986; Furuya *et al.*, 1989). This suggests that the mutations cause only subtle structural changes, increasing the tendency of TTR to form fibrils, such as the formation of a region that is more susceptible to proteolysis (Saraiva & Costa, 1991). X-ray studies of the Met 30 variant of TTR have shown that the molecule is in its near-native state with Cys 10 becoming slightly more exposed (Terry *et al.*, 1993). It has been suggested that this could promote the formation of disulfide bonds between TTR molecules in the process of fibril formation (Thylen *et al.*, 1993).

Five mutation sites exist between residues 71 and 93: (i) a substitution of alanine for valine at position 71, (ii) a substitution of tyrosine for serine at position 77, (iii) the substitutions of serine and asparagine for isoleucine at position 84, (iv) the substitution glutamine for glutamic acid at position 89, and (v) the substitution of asparagine for histidine at position 90, which is a benign substitution. This region lies on the outer surface of the protein and is of particular interest because it contains the one helical structure in this primarily β-sheet protein. Ser 77 occurs within the helix and Ile 84 occurs in the turn following the helical region. Glu 89 is positioned just before the N-terminus of β-strand F, and His 90 and Val 71 occur in the centers of β-strands F and E, respectively. It is possible that this helical moiety plays an important role in stabilizing TTR and that these mutations result in improperly formed structures which are more susceptible to forming amyloid.

In the current study the fragment from residue 71 to residue 93 (TTR 71–93) has been synthesized to investigate the importance of the region to the integrity of transthyretin. NMR spectroscopy has been used to characterize its intrinsic structural properties in various solutions, allowing its importance in the folding of the native protein to be evaluated. The possibility that the peptide could be directly involved in amyloid formation was also considered. As has been reported for the amyloid β-A4 peptide, helix–sheet transitions may occur in amyloid formation (Zagorski & Barrow, 1992). An analogous transition in TTR 71–93 would have important implications for the modeling of TTR in its fibrillar state. Fibril formation was, therefore, monitored in solutions of TTR 71–93 and TTR 105–115 [a control peptide known to form amyloid (Gustavsson *et al.*, 1991)] using electron microscopy.

MATERIALS AND METHODS

Peptide Synthesis and Preparation. TTR 71–93 and TTR 105–115 were synthesized on an Applied Biosystems Model 430A synthesizer by solid-phase methods (Merrifield, 1963). The peptides were purified using a Waters radial diffusion reversed-phase cartridge and LC 1500 HPLC system (ICI Instruments) using a 40-min 0–60% acetonitrile gradient in water and 0.01% trifluoroacetic acid. Amino acid analysis and analytical HPLC confirmed the purity of the samples. Acetonitrile was of HPLC grade (Ajax chemicals). Other chemicals were of reagent grade (Sigma chemicals) and were used without further purification. The amino acid sequences were as follows: TTR 71–93, Val-Glu-Ile-Asp-Thr-Lys-Ser-Tyr-Trp-Lys-Ala-Leu-Gly-Ile-Ser-Pro-Phe-His-Glu-His-Ala-Glu-Val; TTR 105–115, Tyr-Thr-Ile-Ala-Ala-Leu-Leu-Ser-Pro-Tyr-Ser.

TTR 71–93 was made up for NMR experiments in a 5-mm tube (Wilmad) at a concentration of 10 mM peptide in the following solvent systems (Cambridge Isotope Laboratories): deuterated dimethyl sulfoxide (DMSO-d_6), water (i.e., D_2O and 10% D_2O/90% H_2O), and 20% deuterated trifluoroethanol (TFE). All solvent percentages are by volume. The pH in aqueous solutions was 3–4. The sample was recovered between experiments by freeze-drying.

Electron Microscopy. Solutions (10 mg/mL) of the TTR 71–93 and TTR 105–115 were dissolved in (i) water, (ii) 20% acetonitrile, (iii) 10% acetic acid, and (iv) 10% acetic acid neutralized to pH 7 with NH_3. The samples were kept at room temperature and examined the next day and several weeks later by transmission electron microscopy. Aliquots for electron microscopy were placed on butvar-98 coated copper or nickel grids and negatively contrasted with 2% uranyl acetate. Transmission electron microscopy was conducted on a Jeol 100S instrument.

NMR Experiments. ^1H NMR spectra were recorded on Bruker AMX 300, 500, and 600 spectrometers. Two-dimensional (2D) NMR spectra were recorded in the phase-sensitive mode using time-proportional phase incrementation for quadrature detection in the t_1 dimension (Wuthrich *et al.*, 1983). The water proton signal was suppressed by low-power irradiation during the relaxation delay (1.5 s) and during the mixing time of NOESY experiments. NOESY experiments acquired for aqueous samples (10% D_2O) employed a jump–

return pulse (Plateau & Gueron, 1982) in place of the final 90° pulse in the sequence to avoid excitation of the water resonance. Low-temperature studies employed a temperature-controlled stream of cooled air (Haake SK 107 thermostatic bath). Spectra were referenced to residual solvent peaks, calibrated externally using 4,4-dimethyl-4-silapentane-1-sulfonate (DSS). The residual proton signal of DMSO-d_6 was referenced to 2.49 ppm, and aqueous solutions at 25 °C were referenced to water at 4.79 ppm.

One-dimensional spectra were recorded at 5 °C increments at 300 MHz over a temperature range of 25–45 °C, with 16 384 complex data points. The best peak resolution in the NH region was observed at 30 °C in the DMSO-d_6 solution and at 25 °C in water solutions. Most 2D experiments were run at these respective temperatures. Temperature coefficients for the chemical shifts of the amide protons and $^3J_{HN-H\alpha}$ coupling constants were measured primarily from these spectra.

TOCSY experiments were recorded using an MLEV-17 mixing scheme (Bax & Davis, 1985). Mixing times of 120 ms were generally used, but an 80-ms mixing time experiment was run for the peptide in DMSO-d_6 to optimize the intensity of short-range cross-peaks. TOCSY experiments were run at several temperatures, when necessary, to assign overlapped NH shifts for the measurement of temperature coefficients.

Double-quantum-filtered (DQF) COSY experiments (Rance *et al.*, 1983) allowed the accurate measurement of proton shifts and were also used to measure $^3J_{NH-\alpha H}$ coupling constants which were not resolved in the 1D spectra (Marion & Wuthrich, 1983). Coupling constant values from these spectra were corrected for the line-width contributions of the dispersive peaks using an in-house peak deconvolution routine which fitted overlapping Lorentzian lines to the experimental spectra. Phase-sensitive NOESY experiments were acquired at 600 MHz with mixing times of 100 and 250 ms.

2D experiments were collected over 4096 complex data points. Usually 512 increments of 32 scans were acquired over a spectral width corresponding to 11 ppm for both dimensions. Up to 64 scans per increment were acquired for less sensitive NOESY experiments, and only one scan per increment was required for diagnostic TOCSY experiments. Up to 800 increments were collected for improved resolution in the t_1 dimension in the COSY and NOESY experiments.

The data were processed on a Silicon Graphics (SGI 4D/30) computer using the Felix 1.0 software package (Hare Research, Inc). The t_1 dimension was zero-filled to 4096 real data points, with both dimensions being multiplied by a sine-bell function shifted by 90° prior to Fourier transformation. A different window function with a Gauss/Lorentz function coefficient of 0.15 and line broadening of –4 Hz was applied to some NOESY spectra to improve peak resolution. Polynomial baseline correction was used in selected regions to improve the appearance of the spectrum.

NOE cross-peak intensities were measured using the integration function within Felix. These were calibrated relative to the volume of tryptophan aromatic cross-peaks and classified as strong, medium, and weak, corresponding to interproton distance restraints of 1.8–2.7, 1.8–3.5, and 1.8–5.0 Å, respectively (Clore *et al.*, 1986). Appropriate pseudo-atom corrections were applied to nonstereospecifically assigned methyl and methylene protons (Wuthrich *et al.*, 1983).

Structure Calculations. Three-dimensional structures were determined using the experimentally observed NOE constraints in a simulated annealing and energy minimization protocol. These calculations were made with the program XPLOR (Version 3.0; Brunger, 1992) on a personal Iris 4D/30 workstation (Silicon Graphics Inc., Mountain View, CA). In the simulated annealing stage of the calculation (Nilges *et al.*, 1988) 62 inter- and 58 intra-NOE distance constraints were applied to a template structure with randomized ϕ and ψ angles and extended side chains to generate a set of 30 structures. For final refinement, a restrained Powell energy minimization was applied to each structure using a force field based on that of the program CHARMM (Brooks *et al.*, 1983). Structure superpositions were accomplished using Insight (Biosym) on a 4D/220 GTX workstation.

RESULTS

Amyloid Formation. Previous reports of *in vitro* amyloid-like fibril formation have described the solution conditions required for the formation of several peptide- and protein-based fibrils (Gustavsson *et al.*, 1991; Kirschner *et al.*, 1987; Colon & Kelly, 1992). Amyloid-like fibril formation has been found to be concentration dependent and, in some cases, pH dependent (Barrow *et al.*, 1992). Hence the following solution conditions were examined for fibril formation using electron microscopy: 10 mg/mL solutions of TTR 71–93 and TTR 105–115 in (i) water, (ii) 20% acetonitrile, (iii) 10% acetic acid, and (iv) 10% acetic acid adjusted to pH 7 with NH_3. The control peptide TTR 105–115 was insoluble in water, but in 20% acetonitrile fibrils formed that could be detected within 1 day of the preparation. TTR 71–93 did not form amyloid-like structures under any of the solution conditions. Electron microscopy revealed only some amorphous aggregate in a preparation of 10 mg/mL acetic acid after several weeks (Figure 3).

NMR Structural Study. Several solvent systems were examined in this study since the microenvironment of a peptide fragment in a large protein is not necessarily aqueous. The surrounding functionalities in the native protein may exclude a surface from water or compete for hydrogen-bonding or charge interactions. NMR studies were undertaken for TTR 71–93 in DMSO-d_6, in water, and in 20% TFE. Experiments at 25 and 10 °C in water are described.

The NMR spectra showed that the sample was of high purity. No deterioration of the sample or loss of signal was detected over time, nor were chemical shift changes or increases in line width observed for preparations of differing concentrations (1–10 mM). It was concluded that aggregates were not present in the samples studied. This was confirmed from CD spectra, which showed no change over a 10-fold dilution from 1 mM.

Assignment of ^1H Shifts. All intraresidue resonances were assigned from the TOCSY and DQF-COSY spectra by identifying the systems of spin–spin-coupled resonances belonging to a particular amino acid residue. Figure 4 illustrates the TOCSY spectrum for TTR 71–93 in 20% aqueous TFE. Sequential assignments were made using the 2D NOESY spectrum to locate sequential $d_{\alpha N}(i,i+1)$ and $d_{NN}(i,i+1)$ connectivities (Figures 5 and 6). The same procedure was used to assign ^1H resonances in the three solvents studied. Assignments for the ^1H resonances in 20% aqueous TFE, 25 °C, are summarized in Table I.

The deviation of αH shifts from their "random-coil" values (Wuthrich, 1976; Wuthrich, 1986) has been shown to bear a strong relationship to protein secondary structure (Szilagyi & Jardetzky, 1989; Wishart *et al.*, 1992). In particular, it has been found that upfield shifts are experienced by αHs in a helical conformation and comparable downfield shifts are seen for β-strand (extended) conformations. Figure 7 shows

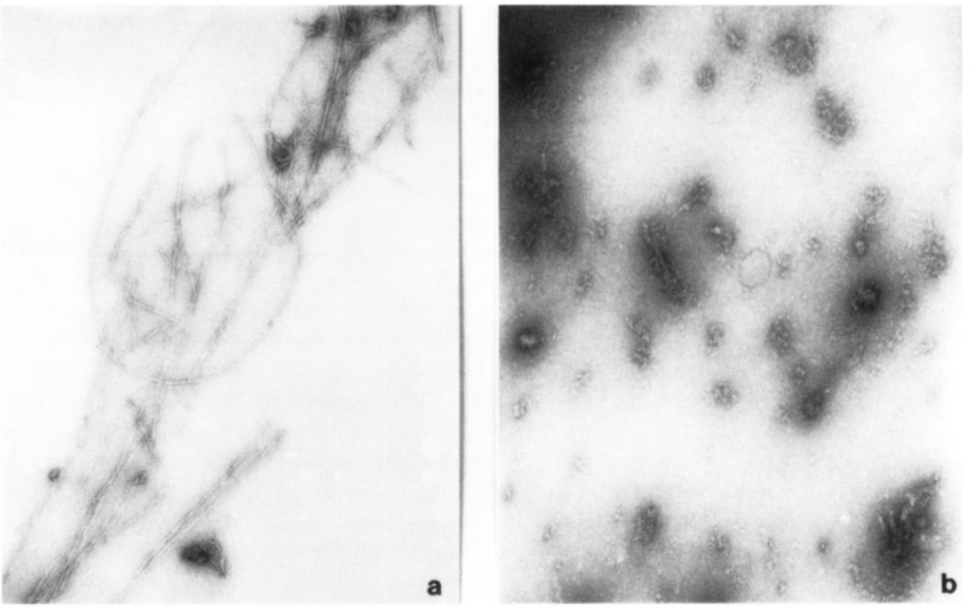

FIGURE 3: Electron micrographs of (a) TTR 105–115 and (b) TTR 71–93 peptide preparations. TTR 71–93 dissolved in 10% acetic acid showed only some amorphous aggregate after several weeks, whereas TTR 105–115 formed fibrils in 20% acetonitrile overnight (magnification 40000×; reproduced at 85% of original figure).

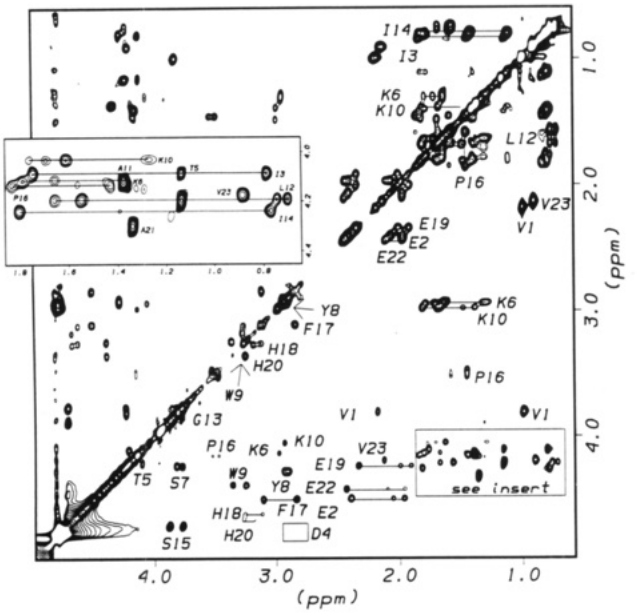

FIGURE 4: Region of a 120-ms TOCSY NMR spectrum of TTR 71–93 (20% TFE, 25 °C, 600 MHz) showing assignments of intraresidue side-chain connectivities. The D4 box indicates the position of the weak D4 αH–βH cross-peak, which can be seen on the other side of the diagonal.

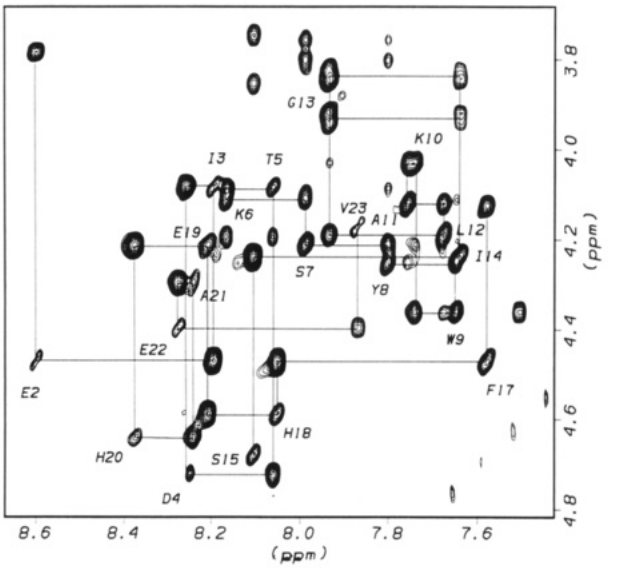

FIGURE 5: NH–αH region of a 250-ms NOESY NMR spectrum of TTR 71–93 (20% TFE, 25 °C, 600 MHz) showing intraresidue and sequential NH to αH connectivities and several of the medium-range connectivities discussed.

the deviations of the αHs from their random-coil values under the three solution conditions. For this study Wuthrich's values for random-coil shifts were used. Although the random-coil shifts by Wishart *et al.* are different, the determination of secondary structure according to their protocol also results in a prediction of helix from residues 5 to 12 (Wishart *et al.*, 1991, 1992). The αH chemical shifts are close to the random-coil values in DMSO-d_6. In water there is some indication of upfield shifts between residues 4 and 12 which becomes very pronounced in 20% TFE. Hence there is increasing helix formation with this progression of solution conditions. No trend toward downfield shifts was observed along the peptide sequence.

NOE Connectivities. While chemical shifts provide a guide to secondary structure, the observation of a direct NOE between a given pair of protons provides much stronger evidence for the presence of a conformer in which a particular interproton distance is maintained. The determination of a significant number of interproton distance restraints from NOE data allows the three-dimensional conformation in solution to be calculated. However, many linear peptides exist in a rapidly fluctuating set of conformations that includes random or extended forms (Dyson & Wright, 1991). In these cases NOE cross-peaks may represent the averaged signal of several conformers, and any analysis of experimental NOE data should take this possibility into account.

The sequential, intraresidue αH–NH, and medium-range NOEs for TTR 71–93 observed under four sets of solution conditions are summarized in Figure 8. In each solvent $d_{\alpha N}(i,i+1)$ NOEs were observed, although spectral overlap prevented some NOEs from being detected. The observation of strong $d_{\alpha N}(i,i+1)$ relative to $d_{\alpha N}(i,i)$ cross-peaks indicates a tendency toward extended chain structures (Dyson *et al.*, 1988a,b). This is the case in DMSO-d_6 and water in the

Table I: Proton Chemical Shifts (ppm) of TTR 71–93 in 20% TFE at 25 °C (Relative to DSS)

residue	NH	αH	βH	other
Val 1		3.80	2.18	γCH_3 0.98
Glu 2	8.62	4.49	2.06, 1.97	γCH_2 2.40
Ile 3	8.21	4.10	1.76	γCH_2 1.40, 1.11; γCH_3 0.80; δCH_3 0.82
Asp 4	8.27	4.74	2.89, 2.78	
Thr 5	8.08	4.10	4.21	γCH_3 1.16
Lys 6	8.19	4.13	1.81, 1.68	γCH_2 1.39; δCH_2 1.47; ϵCH_2 2.98
Ser 7	8.01	4.23	3.82, 3.78	
Tyr 8	7.82	4.27	2.94, 2.90	2,6H 6.72; 3,5H 6.55
Trp 9	7.67	4.38	3.36, 3.25	2,6H 7.20; 4H 7.52; 5H 7.07; 7H 7.45; NH 10.01
Lys 10	7.76	4.05	1.68, 1.61	γCH_2 1.30; δCH_2 1.63; ϵCH_2 2.93
Ala 11	7.76	4.14	1.40	
Leu 12	7.70	4.21	1.68, 1.56	γCH 1.56; δCH_3 0.77, 0.73
Gly 13	7.96	3.95, 3.86		
Ile 14	7.66	4.25	1.82	γCH_2 1.41, 1.10; γCH_3 0.77; δCH_3 0.78
Ser 15	8.13	4.70	3.88, 3.78	
Pro 16		4.15	1.85, 1.59	γCH_2 1.43; δCH_2 3.53, 3.48
Phe 17	7.60	4.49	3.11, 2.84	2,6H 7.15; 3,5H 7.29; 4H 7.25
His 18	8.07	4.61	3.26, 3.11	2H 8.57; 4H 7.24
Glu 19	8.23	4.23	2.00, 1.91	γCH_2 2.34
His 20	8.39	4.66	3.26, 3.17	2H 8.57; 4H 7.29
Ala 21	8.27	4.32	1.36	
Glu 22	8.30	4.42	2.10, 1.96	γCH_2 2.45
Val 23	7.89	4.20	2.13	γCH_3 0.90

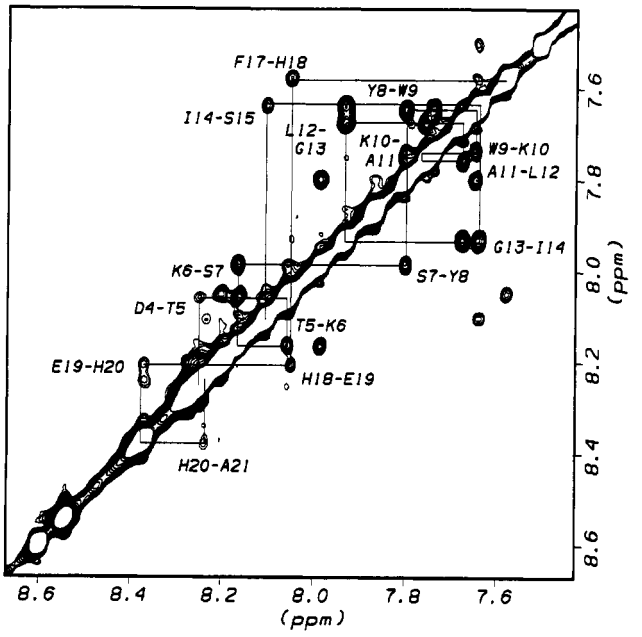

FIGURE 6: NH region of a 250-ms NOESY NMR spectrum of TTR 71–93 (20% TFE, 25 °C, 600 MHz) showing the sequential NH_i to NH_{i+1} connectivities and their relatively high intensities between residues 5 and 14.

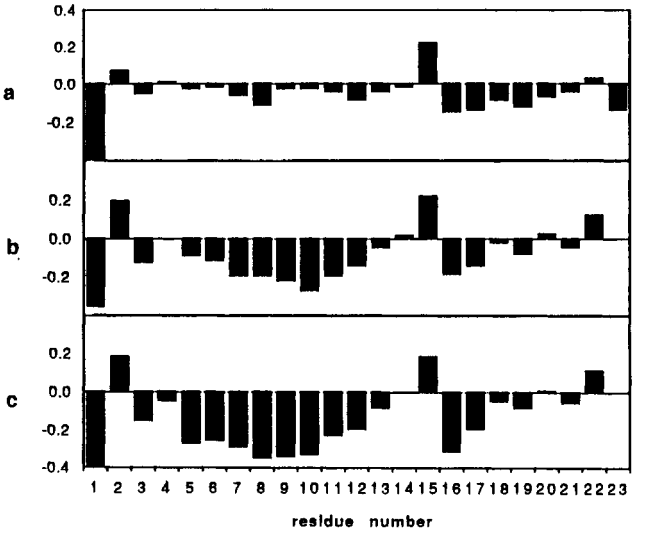

FIGURE 7: Deviation of TTR 71–93 αH shifts from their random-coil values in (a) DMSO-d_6, (b) 10% D_2O, and (c) 20% TFE at 25 °C. The upfield trend between residues 5 and 13 is observed in water and intensifies upon the addition of TFE. Shifts in water and 20% aqueous TFE were compared to random-coil values in water (Wuthrich, 1978), while those in DMSO are relative to random-coil DMSO values (Wuthrich, 1976).

region from residues 5 to 12. In 20% TFE, however, $d_{\alpha N}(i,i)$ cross-peaks are more intense than the $d_{\alpha N}(i,i+1)$ cross-peaks in this region, consistent with an increased population of α-structures through this span in the presence of TFE.

$d_{\beta N}(i,i+1)$ NOEs are observed along most of the sequence in DMSO-d_6, with an increase in intensity near residues 8–10. Fewer of these connectivities were observed in water at 25 °C, but at 10 °C a more complete set of $d_{\beta N}(i,i+1)$ NOEs was observed. In 20% TFE at 25 °C nearly all of the $d_{\beta N}(i,i+1)$ connectivities were observed, and those between residues 5 and 10 were most intense. These signals may be indicative of a greater degree of structural ordering of backbone and side chains in the region.

Many $d_{NN}(i,i+1)$ NOEs were observed under all solution conditions. In 20% TFE these NOEs are particularly strong relative to the $d_{\alpha N}(i,i+1)$ NOEs between residues 5 and 13. Such a pattern is indicative of a helical conformation where sequential NHs are held in close proximity to one another (Bradley *et al.*, 1990). As reflected in the deviations of αHs from random-coil chemical shifts, the trend toward a significant helical population in this region is clearly strongest in the 20% TFE spectra. $d_{NN}(i,i+1)$ connectivities occurring in the DMSO-d_6 spectra are also more intense in the regions about residues 5 and 15 although there is no indication of a helical conformation from the DMSO-d_6 αH shifts.

In DMSO-d_6 several very weak $d_{\alpha\alpha}(i,i+1)$ NOE connectivities were observed; however, they were not observed in NOESY spectra of aqueous systems. While the possibility that these NOEs result from spin diffusion transmitted *via* intervening amide protons cannot be excluded, $d_{\alpha N}(i,i+2)$ NOE connectivities were also observed near the same positions along the sequence, indicating the possibility of turn loci at these positions. Thus a tendency toward partial turns exists for TTR 71–93, among a primarily unstructured ensemble of molecules in DMSO-d_6.

FIGURE 8: Summary of NOE connectivities measured for TTR 71–93 under several solution conditions: (a) DMSO-d_6, 25 °C, (b) 10% D_2O, 25 °C, (c) 10% D_2O, 10 °C, and (d) 20% TFE, 25 °C. The intensities of NOE cross-peaks are indicated by the thickness of the line, grouped into strong, medium, and weak. Overlapping, and therefore ambiguous, cross-peaks are indicated by an asterisk. Absent protons are marked with shaded regions.

No medium-range NOE connectivities were observed for TTR 71–93 in 10% D_2O at 25 °C. At 10 °C, however, at which both the correlation time of the molecule and the mole fraction of stabilized conformer are likely to be increased, $d_{\alpha N}(i,i+3)$ connectivities were clearly identified. Upon the addition of 20% TFE to the aqueous solution a large number of medium-range connectivities were observed, even at 25 °C. These included $d_{\alpha\beta}(i,i+3)$ connectivities, as well as a complete set of $d_{\alpha N}(i,i+3)$ NOEs between residues 5 and 12. These NOEs outline definitively the extent of helix formation in a significant population of conformers. This region of the peptide corresponds precisely to the extent of helix existing in native TTR. $d_{\alpha N}(i,i+2)$ NOEs were also observed between residues 10 and 13. These restraints could represent helix fraying, an irregular helix conformation, or the start of a turn at this point of the structure since this distance is about 4.7 Å in regular helix.

Table II: $^3J_{\alpha H-NH}$ Coupling Constants (Hz) for TTR 71–93 in Three Solvent Systems[a] (10 mM Peptide, 25 °C)

residue	DMSO	water	TFE	residue	DMSO	water	TFE
Glu 2	7.8	7.2	6.7	Gly 13	6.0	6.2	6.0
Ile 3	8.5	6.7	6.8	Ile 14	8.7	8.4	7.0
Asp 4	7.6	7.1	7.5	Ser 15	7.8	5.9	6.6
Thr 5	6.7	6.9	6.2	Phe 17	7.5	6.7	6.9
Lys 6	8.0	6.8	6.8	His 18	6.8	8.2	6.2
Ser 7	8.0	6.4	5.8	Glu 19	8.4	7.9	7.5
Tyr 8	8.2	6.3	5.7	His 20	6.5	5.9	5.5
Trp 9	7.9	6.0	7.0	Ala 21	6.7	6.7	7.5
Lys 10	8.1	6.3	5.7	Glu 22	8.0	6.8	7.5
Ala 11	6.7	6.5	5.9	Val 23	8.3	8.1	7.7
Leu 12	7.7	6.3	6.9				

[a] DMSO, DMSO-d_6; water, 10% D_2O; TFE, 20% TFE.

There was no indication from chemical shifts, from amide exchange data, or from the presence of long-range NOEs of β-sheet formation between the ends of the peptide, as exists in the corresponding region of the native protein. This suggests that the propensity for helix formation in the isolated fragment is much greater than any propensity for β-sheet. The result agrees well with the recent reports by Dyson *et al.*, which showed that fragments from a helical protein, myohemerythrin, had a high probability of forming α-helix as isolated fragments in solution, while fragments from a β-sheet protein, plastocyanin, were usually random coil (Dyson *et al.*, 1992a,b).

$^3J_{\alpha H-NH}$ Coupling. The $^3J_{\alpha H-NH}$ coupling constant expected for α-helix is of the order of 4 Hz and for regular β-strand is about 9 Hz (Wuthrich, 1986). However, it is not unusual to see the conformationally averaged value of 6–7 Hz even for systems with significant populations of structured species (Dyson & Wright, 1991). $^3J_{\alpha H-NH}$ coupling constants for TTR 71–93 ranged between 5.5 and 8.6 Hz in both water and 20% TFE, averaging 6.4 Hz (Table II). Marginally higher values were observed in DMSO-d_6, with $^3J_{\alpha H-NH}$ couplings averaging 7.3 Hz. These results indicate that in aqueous solutions the populations of α-helix- or β-strand-containing species are not apparent from the averaged $^3J_{\alpha H-NH}$ couplings. In DMSO-d_6, however, the higher values reflect the tendency toward a random-coil conformation in this solvent (Pardi *et al.*, 1984).

Hydrogen Bonding. Proteins containing hydrogen bond stabilized structures are frequently characterized by their slow amide proton exchange rates and diminished amide chemical shift temperature gradients (Dyson & Wright, 1991). Upon transfer of the peptide to D_2O, NH exchange was complete within half an hour. In 20% TFE/D_2O, however, several NHs exchanged more slowly and were observable after 40 min. The residual signals corresponded to residues 9, 10, 11, 12, and 14. Due to overlap there was some ambiguity in determining whether all of these NHs were slowly exchanging, but it is striking that the NHs of residues 9–12 are precisely those expected to be involved in hydrogen bonding in a helix from residues 5 to 12.

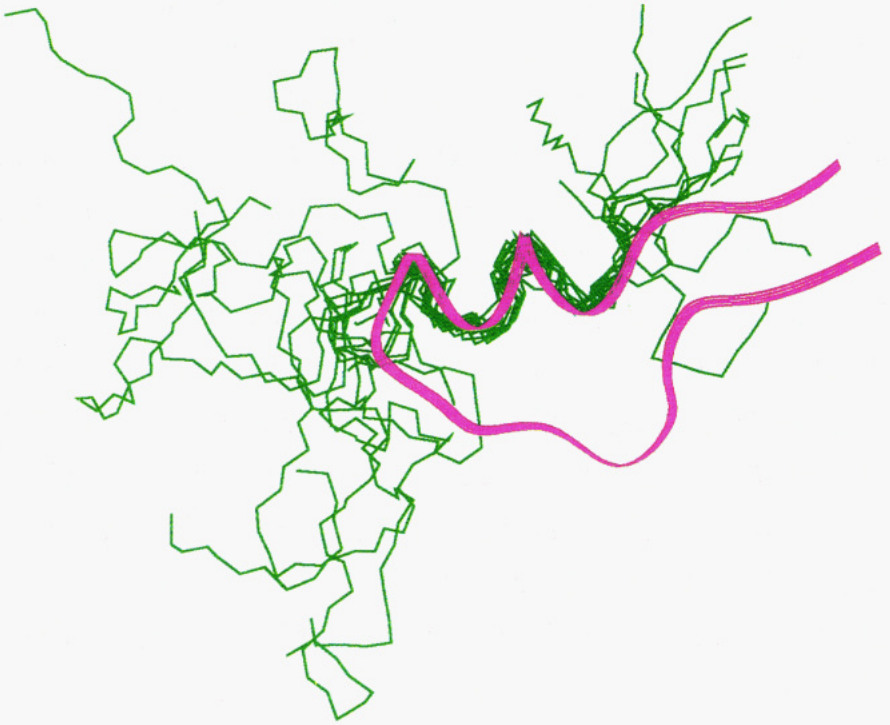

FIGURE 9: Superposition of the backbone (N, αC, C) atoms of 10 structures obtained from XPLOR simulated annealing calculations and crystal coordinates of fragment 71–93 from native TTR. The structures are best fitted to the helical region residues 5–12. The correlation of the position of the helix is clearly evident. No structural restraint is observed for the rest of the molecule.

Temperature coefficients were measured for the amide proton shifts under the three solution conditions. The coefficients were generally greater than 5 ppb/°C, and there was no correlation of low-temperature gradients (<4 ppb/°C) with the slower exchanging NHs. While temperature coefficients may show parallels with amide exchange rates, it is not uncommon to observe high-temperature coefficients for slowly exchanging amide protons (Reed *et al.*, 1988). Generally, less reliance may be placed on temperature coefficients as markers of hydrogen bonding as these may be influenced by additional factors, including chemical shifts of individual conformers (Andersen *et al.*, 1992).

Simulated Annealing and Energy Minimization Using NOE Distance Restraints. The NMR data indicate that while TTR 71–93 may exist predominantly in a disordered form in DMSO-d_6 and water, a significant population of structures containing α-helix persists in 20% TFE. In an attempt to quantitate the helical content of peptides, Bradley *et al.* derived two expressions to calculate the fraction of helical over extended forms. In one of these equations the ratio of NOESY $d_{NN}(i,i+1)$ and $d_{\alpha N}(i,i+1)$ cross-peaks is used, and the second expression estimates the populations from $^3J_{\alpha N}$ values (Bradley *et al.*, 1990). The NOESY (100-ms mixing time) data suggested that the helical content is >80% over residues 5–12 in 20% TFE while the coupling data suggest that the helical content is approximately 65%. While this approach to predicting helical content is based on rather simplified assumptions, it does suggest that the greater part of the population exists in a defined conformation. It was therefore felt that a structure calculation based on the set of NOEs obtained for TTR 71–93 in 20% TFE was justified. It was rationalized that if the NOE distance restraints were inconsistent with a single predominant conformation, poorly defined and nonconverged structures would be produced by the simulation.

A family of 30 structures was calculated using the NOE-based interproton distance restraints in a simulated annealing/energy minimization protocol. The derived structures were consistent with the experimental constraints, to well within 0.1 Å in most cases. Only five NOEs violated by more than 0.5 Å over the total of 30 structures calculated. Superimposition of the backbone atoms of the structures clearly showed convergence to a common helical structure in the region from residue 5 to residue 12 (backbone pairwise RMSD, 1.84 Å). Positions beyond the helical region were essentially randomly scattered. Figure 9 shows a superposition of the ten lowest energy structures overlayed with the corresponding region from the crystal structure of TTR. The set of structures serves to illustrate the concordance of the positioning of the helix with its positioning in the native structure of TTR and to confirm that the NOE distance constraints are consistent with a helix in this region.

DISCUSSION

Although early studies of short linear peptides suggested that they did not exhibit well-defined secondary structure in water (Epand & Sheraga, 1968; Howard *et al.*, 1975; Taniuchi & Anfinsen, 1969; Hermans & Puett, 1971), this may have been because the populations of the folded conformations were small and measurements of structure were strongly influenced by populations of unstructured species. The sensitive techniques of 2D NMR spectroscopy and antibody binding have since identified peptides with a high folding propensity in aqueous as well as organic solutions (Lerner, 1984; Wright *et al.*, 1988).

Stable structures for cyclic and linear peptides have been identified in organic solutions (Ni *et al.*, 1992; Kessler *et al.*, 1988; Wynants *et al.*, 1988; Loosli *et al.*, 1985), but it is clear that solvent interactions play a considerable role. DMSO-d_6 is generally believed to destabilize all but highly preferred conformations through strong polar interactions (Jackson & Mantsch, 1991). The longer correlation time observed for peptides the size of TTR 71–93 in DMSO-d_6, however, means that often NOESY cross-peaks can be observed in DMSO-d_6

which are not detectable in aqueous systems at room temperature.

There are numerous examples of helical structures of varying degrees of stability in water and TFE–water solutions (Bierzynski *et al.*, 1982; Kim & Baldwin, 1984; Shoemaker *et al.*, 1985, 1987; Rico *et al.*, 1986; Dyson *et al.*, 1988a,b). TFE solutions have proven useful for the characterization of helical regions in peptides because while this solvent will not induce helix in a peptide lacking an intrinsic helical tendency, it does act to stabilize a nascent helix (Dyson *et al.*, 1988b). Whether TFE mixtures are a good mimic of a peptide's native environment is still being evaluated (Sonnichsen *et al.*, 1992).

The structural properties of TTR 71–93 under the solution conditions investigated are very much in accordance with these previously reported trends. The existence of nascent helix between residues 5 and 12 of TTR 71–93 in 10% D_2O was evident, and the addition of TFE to the aqueous solution of TTR 71–93 clearly stabilized the helical conformation. The helix corresponds precisely with the position of the helix in the native protein, providing a striking example of intrinsic secondary structure within a region of a protein (Figure 9). The presence of aspartic acid at position 4, which is reported to have a high helix initiation potential, and the helix breaker Gly at position 13 would, perhaps, help to rationalize this observation (Richardson & Richardson, 1988). In DMSO-d_6 only small populations of conformers containing turns were observed, among mainly random-coil conformations.

The antiparallel β-sheet motif that exists in native TTR between residues 71 and 73 and 89 and 93 was not observed in the peptide under any of the solution conditions examined. Although three of the interstrand hydrogen bonds that exist between the ends of fragment 71–93 in the native TTR structure could have formed, there was clearly insufficient driving force for this conformation to persist for any significant period. As noted by Dyson *et al.*, β-sheet formation is a less commonly observed phenomenon in small linear peptides (Dyson *et al.*, 1992a,b).

The observations that (i) an α-helical segment is strongly maintained but (ii) a β-sheet motif is not, in fragment TTR 71–93, have important implications for our understanding of the mechanism of amyloid formation. As the peptide showed no tendency to form amyloid-like structures, its direct involvement in amyloid formation is deemed unlikely. Mutations in this region may result in a subtly repositioned helix and loop. The destabilized protein may then display a greater propensity for amyloid formation based upon improper protein–protein interactions. The substitutions that occur in other regions of TTR may play similar roles in the pathogenesis of amyloidosis. A further understanding of protein folding and stabilization through studies of protein fragments may provide insight into the phenomena of fibril formation by TTR.

ACKNOWLEDGMENT

We thank Dr. Alan Kirkpatrick (CSIRO Division of Biomolecular Engineering) for synthesizing the peptides. We also thank Barry Veitch (Department of Biochemistry, Monash University) for providing the electron micrographs and Dr. Per Kraulis (Department of Biochemistry, University of Cambridge, Cambridge, U.K.) for the kind donation of his Molscript software package.

REFERENCES

Anderson, N. H., Chen, C., Marschner, T. M., Krystek, S. R., Jr., & Bassolino, D. A. (1992) *Biochemistry 31*, 1280–1295.

Barrow, C. J., Yasuda, A., Kenny, P. T. M., & Zagorski, M. G. (1992) *J. Mol. Biol. 225*, 1075–1093.

Bax, A., & Davis. D. G. (1985) *J. Magn. Reson. 63*, 207–213.

Benson, M. D. (1991) *J. Med. Genet. 28*, 73–78.

Bernstein, F. A., Koetzle, T. F., Williams, G. J. B., Meyer, E. F., Brice, M. D., Rodgers, J. R., Kennard, O., Shimanonouchi, T., &Tamsumi, M. (1977) *J. Mol. Biol. 268*, 535–542.

Bierzynski, A., Kim, P. S., & Baldwin, R. L. (1982) *Proc. Natl. Acad. Sci. U.S.A. 79*, 2470–2474.

Blake, C. C. F., Geisow, M. J., & Oatley, S. J. (1978) *J. Mol. Biol. 121*, 339–356.

Bradley, E. K., Thomason, J. F., Cohen, F. E., Kosen, P. A., & Kuntz, I. D. (1990) *J. Mol. Biol. 215*, 607–622.

Branch, W. T., Robbins, J., & Edelhoch, H. (1972) *Arch. Biochem. Biophys. 152*, 144–151.

Brooks, B. R., Bruccoleri, R. E., Olafson, B. D., States, D. J., Swaminathan, S., & Karplus, M. (1983) *J. Comput. Chem. 4*, 187–217.

Brunger, A. T. (1992) *XPLOR Manual*, Yale University, New Haven, CT.

Clore, G. M., Brunger, A. T., Karplus, M., & Gronenborn, A. M. (1986) *J. Mol. Biol. 191*, 523–551.

Colon, W., & Kelly, J. W. (1992) *Biochemistry 31*, 8654–8660.

Dyson, H. J., & Wright, P. E. (1991) *Annu. Rev. Biophys. Biophys. Chem. 20*, 519–538.

Dyson, H. J., Rance, M., Houghten, R. A., Lerner, R. A., & Wright, P. E. (1988a) *J. Mol. Biol. 210*, 161–200.

Dyson, H. J., Rance, M., Houghten, R. A., Wright, P. E., & Lerner, R. A. (1988b) *J. Mol. Biol. 210*, 201–217.

Dyson, H. J., Merutka, G., Waltho, J. P., Lerner, R. A., & Wright, P. E. (1992a) *J. Mol. Biol. 226*, 795–817.

Dyson, H. J., Sayre, J. R. Merutka, G., Shin, H.-C., Lerner, A. R., & Wright P. E. (1992b) *J. Mol. Biol. 226*, 819–835.

Epand, R. M., & Sheraga, H. A. (1968) *Biochemistry 7*, 2864–2872.

Furuya, H., Nakazato, M., Joao, M., Saraiva, M., Costa, P. P., Sasaki, H., Matsuo, H., Goto, I., & Sakaki, Y. (1989) *Biochem. Biophys. Res. Commun. 163*, 851–859.

Gafni, J., Fischel, B., Reif, R., Yaron, M., & Pras, M. (1985) *Q. J. Med. 55*, 33–43.

Glenner, G. G. (1980) *N. Engl. J. Med. 320*, 1283–1292.

Gustavsson, A., Engstrom, U., & Westermark, P. (1991) *Biochem. Biophys. Res. Commun. 175*, 1159–1164.

Hermans, J., & Puett, D. (1971) *Biopolymers 10*, 895–914.

Howard, J. C., Ali, A., Sheraga, H. A., & Momany, F. A. (1975) *Macromolecules 8*, 607–622.

Jackson, M., & Mantsch, H. M. (1981) *Biochim. Biophys. Acta 1078*, 231–235.

Kessler, H., Bats, J. W., Griesinger, C., Koll, S., Will, M., & Wagner, K. (1988) *J. Am. Chem. Soc. 110*, 1033–1049.

Kim, P. S., & Baldwin R. L. (1984) *Nature 307*, 329–334.

Kirschner, D. A., Inouye, H., Duffy, L. K., Sinclair, A., Lind, M., & Selkoe, D. J. (1987) *Proc. Natl. Acad. Sci. U.S.A. 84*, 6953–6957.

Kraulis, P. J. (1991) *J. Appl. Crystallogr. 24*, 946–950.

Lerner, R. A. (1984) *Adv. Immunol. 36*, 361–344.

Loosli, H.-R., Kessler, H., Oschkinat, H., Weber, H-P., Petcher, T. J., & Widmer, A. (1985) *Helv. Chim. Acta 68*, 682–703.

Marion, D., & Wuthrich, K. (1983) *Biochem. Biophys. Res. Commun. 113*, 967–974.

Merrifield, R. B. (1963) *J. Am. Chem. Soc. 85*, 2149–2154.

Ni, F., Ripoll, D. R., & Purisima, E. O. (1992) *Biochemistry 31*, 2545–2554.

Nilges, M., Gronenborn, A. M., Brunger, A. T., & Clore, G. M. (1988) *Protein Eng. 2*, 27–38.

Pardi, A., Billeter, M., & Wuthrich, K. (1984) *J. Mol. Biol. 180*, 741–751.

Plateau, P., & Gueron, M. (1982) *J. Am. Chem. Soc. 104*, 4310–7311.

Rance, M., Sorenson, O. W., Bodenhausen, G., Wagner, G., Ernst, R. R., & Wuthrich, K. (1983) *Biochem. Biophys. Res. Commun. 117*, 479–495.

Reed, J., Hull, W. E., Lieth, C.-W., Kubler, D., Suhai, S., & Kinzel, V. (1988) *Eur. J. Biochem. 178*, 141–154.

Refetoff, S., Dwulet, F. E., & Besen, M. D. (1986) *J. Clin. Endocrinol. Metab. 63*, 1432–1437.

Richardson, J. S., & Richardson, D. C. (1988) *Science 240*, 1648–1652.

Rico, M., Santoro, J., Bermejo, F. J., Herranz, J., Nieto, J. L., Gallego, E., & Jimenez, M. A. (1986) *Biopolymers 25*, 1031–1053.

Saraiva, M. J. M., & Costa, P. P. (1991) in *Amyloid and Amyloidosis 1990* (Natvig, J., Forre, O., Husby, G., Hesebekk, A., Skogen, B., Bletten, K., & Westermark, P., Eds.) pp 569–574, Kluwer Academic Publishers, Dordrecht, Germany.

Shoemaker, K. R., Kim, P. S., Brems, D. N., Marqusee, S., York, E. J., Chaiken, I. M., Stewart, J. M., & Baldwin, R. L. (1985) *Proc. Natl. Acad. Sci. U.S.A. 82*, 2349–2355.

Shoemaker, K. R., Kim, P. S., York, E. J., Stewart, J. M., & Baldwin, R. L. (1987) *Nature 326*, 563–567.

Sonnichsen, F. D., Van Eyk, J. E., Hodges, R. S., & Sykes, B. D. (1992) *Biochemistry 31*, 8790–8798.

Szilagyi, L., & Jardetzky, O. (1989) *J. Magn. Reson. 83*, 441–449.

Taniuchi, H., & Anfinsen, C. (1969) *J. Biol. Chem. 244*, 3864–3875.

Terry, C. J., Damas, A. M., Oliveira, P., Saraiva, M. J. M., Alves, I. L., Costa, P. P., Matias, P. M., Sakaki, Y., & Blake, C. C. F. (1993) *EMBO J. 12*, 735–741.

Thylen, C., Wahlqvist, J., Haettner, E., Sandgren, O., Holmgren, G., & Lundgren, E. (1993) *EMBO J. 12*, 743–748.

Westermark, P., Sletten, K., Johansson, B., & Cornwell, G. G. (1990) *Proc. Natl. Acad. Sci. U.S.A. 87*, 2843–2845.

Wishart, D. S., Sykes, B. D., & Richards, F. M. (1991) *J. Mol. Biol. 222*, 311–333.

Wishart, D. S., Sykes, B. D., & Richards, F. M. (1992) *Biochemistry 31*, 1647–1651.

Wright, P. E., Dyson, H. J., & Lerner, R. A. (1988) *Biochemistry 27*, 7167–7175.

Wuthrich, K. (1976) in *NMR in Biological Research: Peptides and Proteins*, North-Holland Publishing Co., Amsterdam.

Wuthrich, K. (1986) in *NMR of Proteins and Nucleic Acids*, Wiley & Sons, New York.

Wuthrich, K., Billeter, M., & Braun, W. (1983) *J. Mol. Biol. 169*, 949–961.

Wynants, C., Coy, D. H., & Van Binst, G. (1988) *Tetrahedron 44*, 941–971.

Zagorski, M. G., & Barrow, C. J. (1992) *Biochemistry 31*, 5621–5631.